

Efficient Triplet–Triplet Annihilation-Based Upconversion for Nanoparticle Phototargeting

Weiping Wang^{†,‡,§}, Qian Liu^{†,‡}, Changyou Zhan^{†,‡}, Aoune Barhoumi^{†,‡}, Tianshe Yang,[§] Ryan G. Wylie,^{†,‡} Patrick A. Armstrong,^{†,‡} and Daniel S. Kohane^{*,†,‡}

[†]Laboratory for Biomaterials and Drug Delivery, Department of Anesthesiology, Division of Critical Care Medicine, Boston Children's Hospital, Harvard Medical School, 300 Longwood Avenue, Boston, Massachusetts 02115, United States

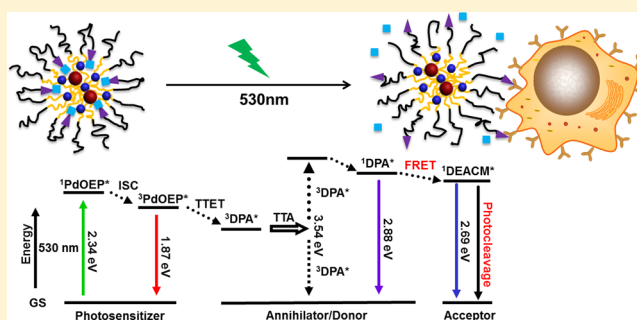
[‡]David H. Koch Institute for Integrative Cancer Research, Massachusetts Institute of Technology, 77 Massachusetts Avenue, Cambridge, Massachusetts 02139, United States

[§]Institute of Advanced Materials, School of Materials Science and Engineering, Nanjing University of Posts and Telecommunications, 9 Wenyuan Road, Nanjing 210023, People's Republic of China

S Supporting Information

ABSTRACT: High-efficiency upconverted light would be a desirable stimulus for triggered drug delivery. Here we present a general strategy to achieve photoreactions based on triplet–triplet annihilation upconversion (TTA-UC) and Förster resonance energy transfer (FRET). We designed PLA–PEG micellar nanoparticles containing in their cores hydrophobic photosensitizer and annihilator molecules which, when stimulated with green light, would undergo TTA-UC. The upconverted energy was then transferred by FRET to a hydrophobic photocleavable group (DEACM), also in the core. The DEACM was bonded to (and thus inactivated) the cell-binding peptide cyclo-(RGDFK), which was bound to the PLA–PEG chain. Cleavage of DEACM by FRET reactivated the PLA–PEG-bound peptide and allowed it to move from the particle core to the surface. TTA-UC followed by FRET allowed photocontrolled binding of cell adhesion with green light LED irradiation at low irradiance for short periods. These are attractive properties in phototriggered systems.

KEYWORDS: Caged ligands, photocleavage, photoresponsive, phototargeted, shielding, upconverting micelles



Stimulus-responsiveness allows spatiotemporal control over nanocarrier targeting and drug release and can therefore enhance therapy while minimizing side effects.^{1,2} We and others have demonstrated the possibility of using light to control the binding of nanocarriers to target cells (phototargeting).^{3–9} Conjugation of a photocleavable group (i.e., caging) deactivates the binding activity of ligands on the nanocarrier surface. Irradiation at the appropriate wavelength removes the caging group and exposes the ligand, enabling binding to target cells. Photocleavage requires short wavelength (high-energy) light, which can cause phototoxicity.^{10,11} However, long-wavelength (low-energy) light that is less toxic cannot trigger photocleavage. Strategies for converting long-wavelength light into short-wavelength light are of interest, because they may allow photocleavage reactions with less phototoxicity. Two-photon absorption^{12,13} and second harmonic generation^{14,15} are examples of approaches that have been employed to trigger UV-sensitive reactions with long-wavelength light. These strategies require the use of high laser irradiances. Lanthanide-based upconversion^{16,17} requires lower irradiances but a coherent light source is still needed.

Triplet–triplet annihilation (TTA) is an upconversion process which has been explored in nonbiomedical photochemical reactions.^{18–22} It can be driven by low-power noncoherent light sources ($\sim\text{mW cm}^{-2}$),^{17,23–26} which enhances safety and is of practical and economic benefit. In TTA-upconversion (TTA-UC; Figure 1a),¹⁷ a low-energy photon is absorbed by a photosensitizer, which then undergoes intersystem crossing (ISC) to form a more stable triplet state. The triplet state energy of the photosensitizer is subsequently transferred to a molecule that is thus excited to its triplet state. Two such molecules in the triplet state can then combine their energies through TTA to form one molecule in the singlet state (with higher energy) and another in the ground state. (Those molecules are termed annihilators because their interaction annihilates the triplet state.) The molecule in the singlet state can relax to the ground state, usually by emission of a higher-energy photon. A key hypothesis of this work is that relaxation

Received: April 5, 2015
Revised: May 23, 2015

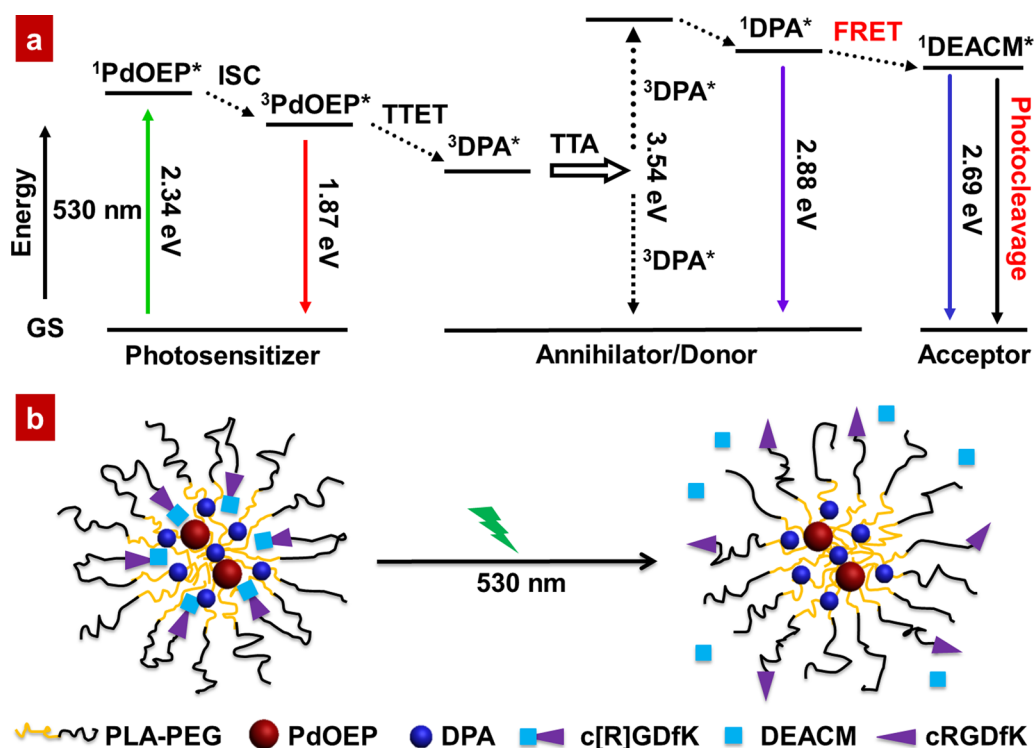


Figure 1. Schematic illustration of TTA-UC and FRET processes. (a) Jablonski diagram illustrating the mechanism of TTA-UC and FRET processes discussed in the text. GS: the ground state. ISC: intersystem crossing. TTET: triplet–triplet energy transfer. TTA: triplet–triplet annihilation. FRET: Förster resonance energy transfer. (b) Schematic of the phototriggering of the polymeric micellar nanoparticle by TTA-UC and FRET.

to the ground state can also be achieved by Förster resonance energy transfer (FRET).

Here we describe an approach whereby TTA-UC is coupled with FRET to create an upconversion-based photoresponsive nanoparticulate system. Incident long-wavelength light is efficiently upconverted to high energy through TTA, and transferred by FRET to a photocleavable group, triggering its cleavage; some of the energy goes to emitting a high-energy photon. Cleavage of that bond removes the photocleavable (caging) group from a targeting ligand, restoring its binding activity (Figure 1b).

We selected palladium octaethylporphyrin (PdOEP, excitation = 532 nm) as the photosensitizer and 9,10-diphenylanthracene (DPA, emission = 400–500 nm) as the annihilator, due to their high upconversion efficiency.²⁷ PdOEP and DPA were encapsulated in the hydrophobic core of a polymeric micelle self-assembled from the block copolymer poly(D,L-lactic acid)-poly(ethylene oxide) (PLA-PEG). The peptide cyclo-(RGDfK) (cRGDfK) was conjugated on the PEG end as the targeting group. cRGDfK was chosen because it binds preferentially to $\alpha_v\beta_3$ integrin, which is overexpressed on tumor cells and angiogenic endothelial cells during tumor growth.^{28,29} Photocaging of this peptide with a 2-nitrobenzyl-based group has been used to regulate cell adhesion with UV light on solid surfaces in vitro and hydrogels in vivo.^{30,31} We selected a coumarin-based group, (7-diethylaminocoumarin-4-yl)methyl (DEACM), as the caging group, because of its high photocleavage efficiency and relatively long absorption wavelength^{32–34} (up to 455 nm, which overlaps with the emission spectrum of DPA, enabling FRET³⁵). We hypothesize that the hydrophobicity of the DEACM would place the DEACM-caged cRGDfK in the PLA core of the PLA-PEG micellar nanoparticles. Because FRET efficiency also depends on the

distance between the donor and the acceptor, typically in the range of 1–10 nm,³⁵ this arrangement (PdOEP, DPA, and DEACM being in the core) would allow TTA-UC energy to be efficiently transferred to the DEACM through FRET (Figure 1), causing the removal of the hydrophobic caging group. Uncaging will allow the hydrophilic peptide to return to the micelle surface, allowing the binding of micelles to target cells.

Results and Discussion. Construction of Phototargeted Polymeric Micelles. The photoresponsive cell-targeting portion of the micellar nanoparticle, DEACM-caged cRGDfK (c[R]-GDfK; Figure 2a), was synthesized and characterized. c[R]-GDfK showed a broad UV–visible absorption spectrum with a peak at 388 nm and a full width at half-maximum (fwhm) of 31 nm (Figure 2b) that overlapped with the TTA-UC emission spectrum from DPA (annihilator/donor; Supporting Information Figure 1), suggesting the possibility of FRET between DPA (donor) and DEACM (acceptor). The DEACM group on the peptide had a fluorescence emission peak at 493 nm (Figure 2b) when excited at 385 nm; this was used below to probe the polarity of the environment surrounding DEACM. Irradiation of c[R]GDfK with a 400 nm light-emitting diode (LED) at 50 mW cm^{-2} for 1 min resulted in cleavage of c[R]GDfK: on high-performance liquid chromatography (HPLC; Supporting Information Figure 2) the c[R]GDfK peak decreased and two new peaks appeared that had the same elution times as free cRGDfK and 7-diethylamino-4-hydroxymethylcoumarin (DEACM-OH). The identity of the peaks was further confirmed by mass spectrometry (Supporting Information Figure 3). Approximately 86% of cleavage occurred within 30 s of irradiation at 50 mW cm^{-2} (Figure 2c). At an irradiance as low as 2.3 mW cm^{-2} , ~42% of c[R]GDfK was cleaved after 2 min of irradiation. The results demonstrate that the photo-

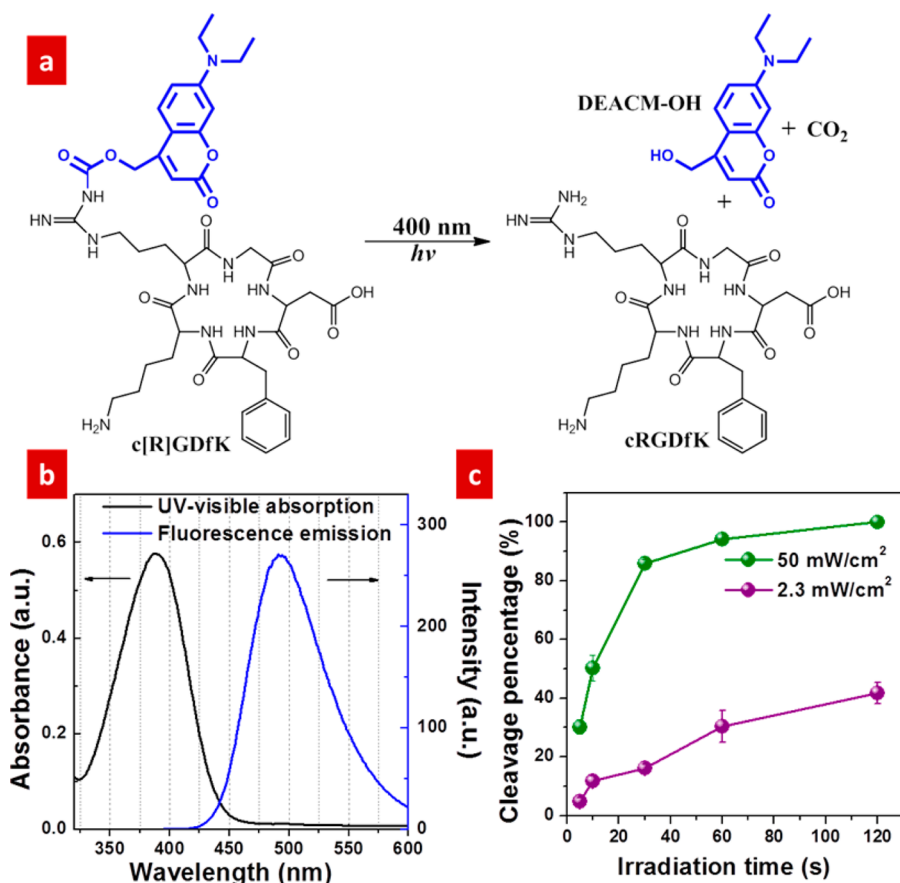


Figure 2. Photocleavage of c[R]GDfK. (a) Photocleavage of c[R]GDfK. DEACM-OH and intact cRGDfK peptide are released upon irradiation at 400 nm. (b) UV-visible absorption and fluorescence emission spectra of c[R]GDfK in PBS (pH 7.4). The excitation wavelength for the fluorescence spectrum was 385 nm. (c) Photocleavage rate of c[R]GDfK in PBS, as determined by HPLC (detected at 390 nm), after continuous irradiation with 400 nm LED light at 2.3 mW cm⁻² and 50 mW cm⁻² (data are means \pm SD; $n = 4$). a.u. = arbitrary units. The concentration of c[R]GDfK in all samples was 50 μ g mL⁻¹.

cleavage reaction could generate intact cRGDfK peptide after short periods of relatively low irradiances.

The c[R]GDfK was conjugated onto block copolymer PLA-PEG to produce PLA-PEG-c[R]GDfK (Supporting Information Figure 4). Phototargeted polymeric micelles were made by the thin-film hydration method from PLA-PEG-c[R]GDfK and PLA-methoxy PEG (mPEG) (1:4 weight ratio).³⁶ The resulting micellar nanoparticles, NP-c[R]GDfK, were dispersible in aqueous solution and had a hydrodynamic diameter of 33.0 nm (Supporting Information Figure 5).

We hypothesized that the hydrophobicity of DEACM would cause it to localize in the PLA core of NP-c[R]GDfK (Figure 3a). That hypothesis was supported by the fact that the fluorescence spectrum of NP-c[R]GDfK (maximum at 464 nm; Figure 3b) was blue shifted in relation to that of free c[R]GDfK in aqueous solution (maximum at 493 nm; Figure 2b), suggesting a change in ambient polarity. This possibility was supported by the finding that the fluorescence spectra of c[R]GDfK showed a clear blue shift with decreasing solvent polarity (Figure 3c). These data indicated that incorporation of DEACM into NP-c[R]GDfK placed it in a less polar environment than that of c[R]GDfK molecules in aqueous solution,³⁷ that is, that the DEACM was not on or in the hydrophilic PEG shell of the micelle but that the PEG block had looped around so that the hydrophobic DEACM³⁸ was in the less polar hydrophobic PLA core (Figure 3a).

According to the proposed structural arrangement, irradiation of NP-c[R]GDfK with 400 nm LED light would release free DEACM-OH, which is more hydrophilic than the conjugated DEACM,³⁸ into the aqueous environment (Figure 3a). This was supported by a red shift and decrease in the emission intensity of NP-c[R]GDfK solution upon irradiation (Figure 3b). The red shift was attributable to the increased polarity of DEACM's environment and the decrease in intensity to the quenching of fluorescence by water.^{37,39}

To further demonstrate that DEACM was localized in the hydrophobic core, DEACM-PLA-mPEG was synthesized (Supporting Information Figure 6), which self-assembled into micellar nanoparticles (NP_{DEACM}; Supporting Information Figures 7 and 8). Because the DEACM group was on the hydrophobic end of the conjugate, it should be located in the PLA core. The emission peak of NP_{DEACM} at 464 nm in PBS (Figure 3d) further supports the view that the DEACM in NP-c[R]GDfK (Figure 3b; emission peak also at 464 nm) was located in the hydrophobic PLA core. Moreover, the difference in the emission peaks of DEACM (Figure 3d) from 464 nm (for NP_{DEACM}) to 494 nm (for DEACM-OH solution) is consistent with the change in the polarity of DEACM's environment from the nonpolar PLA core to aqueous conditions. These results indicate that DEACM is located in the PLA core of NP-c[R]GDfK.

The structure was investigated directly by proton nuclear magnetic resonance (¹H NMR) spectroscopy (Figure 3e). The

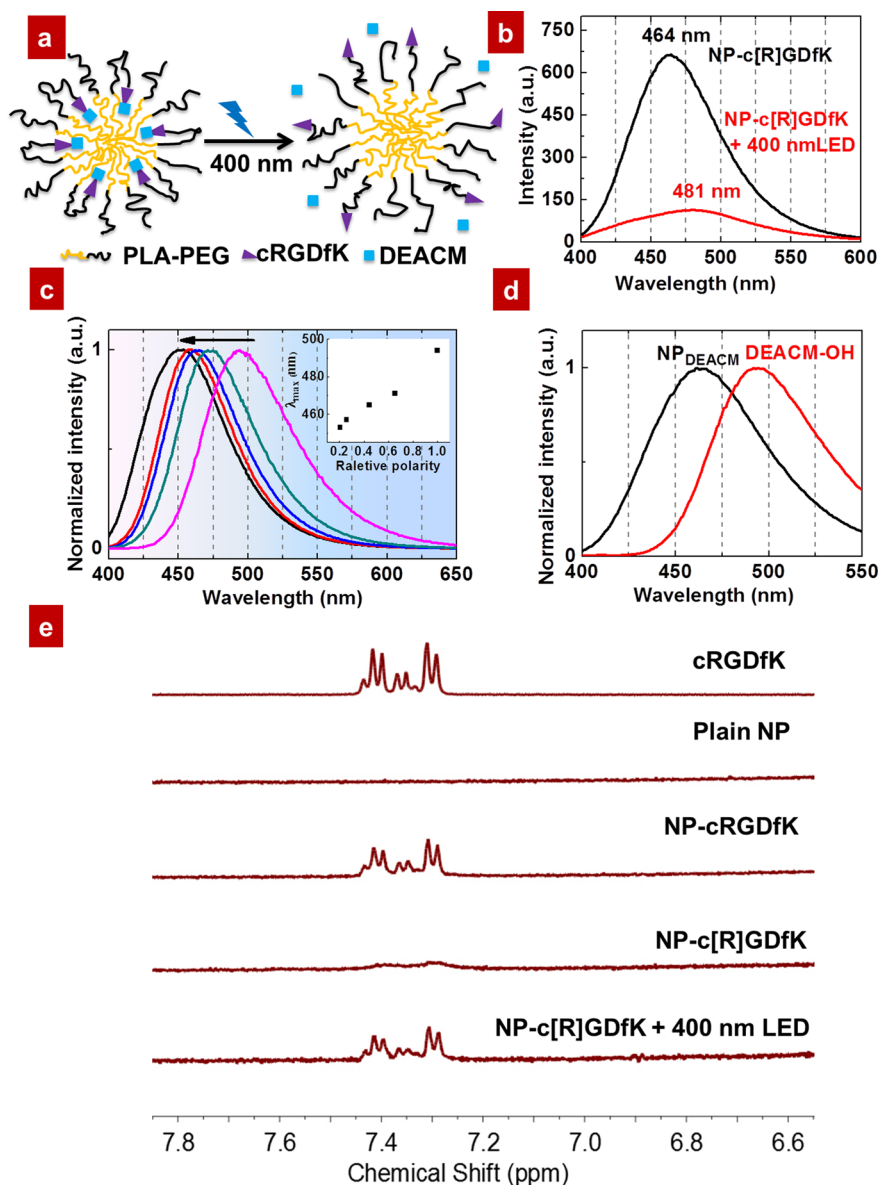


Figure 3. Localization of c[R]GDfK in the hydrophobic core of NP-c[R]GDfK. (a) Schematic of light-triggered activation of c[R]GDfK on NP-c[R]GDfK. (b) Fluorescence emission spectra of NP-c[R]GDfK and NP-c[R]GDfK irradiated for 1 min (50 mW cm^{-2} , 400 nm) in PBS. (c) Fluorescence emission spectra of c[R]GDfK in different solvents, including tetrahydrofuran (THF, polarity relative to water: 0.21), chloroform (CHCl_3 , 0.26), dimethyl sulfoxide (DMSO, 0.44), ethanol (0.65), and water (H_2O , 1.00). The arrow indicates the direction of decreasing solvent polarity. The inset is the plot of the emission maximum (λ_{max}) versus the relative polarity of solvents. (d) Fluorescence emission spectra of NP_{DEACM} (micelles with DEACM on the hydrophobic end of the block polymer) and DEACM-OH in PBS. In panels (c,d), spectra were normalized so that their maximum intensities equaled 1. The excitation wavelength of all fluorescence measurements was 385 nm. (e) ^1H NMR spectra of free cRGDfK and different polymeric micelles in D_2O . Irradiation was done with a 400 nm LED (50 mW cm^{-2} , 1 min).

^1H NMR spectrum of NP-cRGDfK, which was formed with PLA-PEG-cRGDfK (Supporting Information Figure 9) and PLA-mPEG (1:4 weight ratio), in D_2O showed chemical shifts of 7.25–7.45 ppm that were from the resonances of the phenyl protons of cRGDfK (Figure 3e).⁴⁰ Micelles formed with PLA-mPEG only (termed plain NP) did not show those peaks. The ^1H NMR spectrum of NP-c[R]GDfK also did not show those peaks, presumably because of the restricted mobility of the phenyl protons of cRGDfK within the PLA cores of the micelles,⁴⁰ where they were because of DEACM's hydrophobicity. Irradiation at 400 nm resulted in the return of peaks at the same positions as in NP-cRGDfK. These results confirm that the phenylalanine in cRGDfK was located in the PLA core

of NP-c[R]GDfK and that photocleavage would return it to the surface. The absence of the characteristic peaks of DEACM-OH in Figure 3e (NP-c[R]GDfK + 400 nm LED group) is likely because the released DEACM-OH is present at too low concentration to be detected by ^1H NMR. We cannot exclude the possibility that some DEACM-OH remained within the particle core after irradiation.

Photocleavage Triggered by TTA-UC. The photosensitizer PdOEP and the annihilator DPA were incorporated into PLA-mPEG micellar nanoparticles (termed NP_{TTA}) by simple mixing during micelle formation. NP_{TTA} produced upconversion emission (Figure 4a) under irradiation at 532 nm (commercially available green lasers; Supporting Information Figure 10a). At low irradiances, the emission intensity of NP_{TTA}

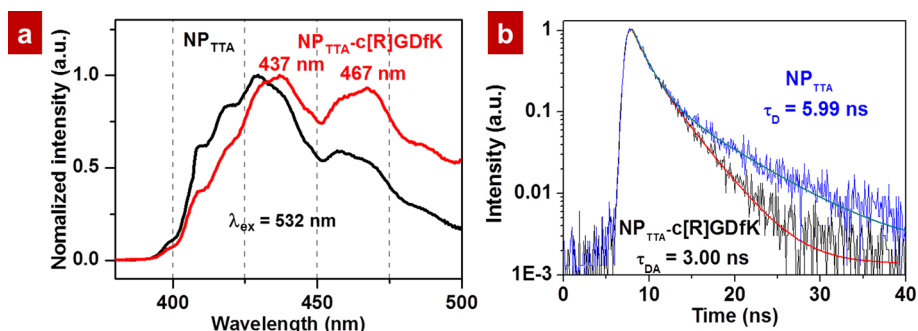


Figure 4. Characterization of the FRET process in $\text{NP}_{\text{TTA}}\text{-c}[\text{R}]\text{GdfK}$. (a) TTA-UC emission spectra of NP_{TTA} and $\text{NP}_{\text{TTA}}\text{-c}[\text{R}]\text{GdfK}$ when excited at 532 nm. Spectra were normalized so that their maximum intensities equaled 1. (b) Decay of fluorescence of DPA in NP_{TTA} and $\text{NP}_{\text{TTA}}\text{-c}[\text{R}]\text{GdfK}$ with excitation at 379 nm and emission at 410 nm. τ is fluorescence lifetime; τ_{DA} = lifetime in the presence of the acceptor DEACM; τ_{D} = lifetime in the absence of the acceptor DEACM.

was proportional to the square of the irradiance and was linear at high irradiances (Supporting Information Figure 10b), a pattern characteristic of TTA-UC.⁴¹ The TTA-UC efficiency¹³ in NP_{TTA} (see Methods in Supporting Information) was 3.8% when irradiated at 532 nm and 150 mW cm^{-2} . (Here, calculation of UC efficiency included multiplication by a factor of 2 to reflect the fact that emission of a single photon required the absorption of two.)

Phototargeted micellar nanoparticles containing PdOEP and DPA (termed $\text{NP}_{\text{TTA}}\text{-c}[\text{R}]\text{GdfK}$) with a hydrodynamic diameter of 36.7 nm (Supporting Information Figure 11) were produced by self-assembly of PLA-PEG- $\text{c}[\text{R}]\text{GdfK}$ and PLA-mPEG (1:4 weight ratio) together with PdOEP and DPA. The analyses of TTA-UC emission spectra and fluorescence lifetimes of DPA (Figure 4) were consistent with FRET between DPA and DEACM in $\text{NP}_{\text{TTA}}\text{-c}[\text{R}]\text{GdfK}$. When irradiated with a 532 nm laser, the TTA-UC emission spectrum of $\text{NP}_{\text{TTA}}\text{-c}[\text{R}]\text{GdfK}$ showed two peaks in the relatively long wavelengths at 437 and 467 nm, that were not present in NP_{TTA} (Figure 4a), indicating that DEACM accepted the TTA-UC energy and emitted fluorescence. The peak at 467 nm could be attributed to the fluorescence of DEACM excited through FRET, because the fluorescence maximum of DEACM inside $\text{NP}\text{-c}[\text{R}]\text{GdfK}$ is around 464 nm (Figure 3b). These changes in the spectrum of NP_{TTA} were not seen with a mixture of NP_{TTA} and free $\text{c}[\text{R}]\text{GdfK}$ in solution (Supporting Information Figure 12), indicating that FRET did not happen, presumably because DEACM was far from the DPA (>10 nm) due to the separation of the PEG (MW 3000) shell (around 10 nm in thickness⁴³) and the free movement of $\text{c}[\text{R}]\text{GdfK}$ molecules in solution.

In general, FRET reduces the fluorescence lifetime of donor fluorophores.^{44,45} In the absence of the acceptor DEACM, the fluorescence lifetime of the donor DPA (τ_{D}) in NP_{TTA} was 5.99 ± 0.04 ns (Figure 4b); in the presence of the acceptor DEACM, the fluorescence lifetime of the donor DPA (τ_{DA}) in $\text{NP}_{\text{TTA}}\text{-c}[\text{R}]\text{GdfK}$ was reduced to 3.00 ± 0.02 ns, indicating the existence of FRET from DPA to DEACM. The FRET efficiency (E) was 49.9%, determined according to eq 1³⁵

$$E = 1 - \frac{\tau_{\text{DA}}}{\tau_{\text{D}}} \quad (1)$$

where E indicates the percentage of excitation photons that contribute to FRET. These results demonstrate the occurrence of FRET in $\text{NP}_{\text{TTA}}\text{-c}[\text{R}]\text{GdfK}$ from DPA to DEACM, as illustrated in Figure 1b. Although a role for reabsorption in the

energy transfer from DPA to DEACM cannot be ruled out, FRET played the major part, given that transfer by reabsorption is orders of magnitude less efficient than FRET.⁴⁶

Photocleavage of DEACM from $\text{NP}_{\text{TTA}}\text{-c}[\text{R}]\text{GdfK}$ was assessed by irradiating the micelles with a 530 nm LED in PBS, separating the free DEACM-OH from the micelles by centrifugal filtration (50 000 Da cutoff), and analyzing the filtrate by HPLC. The filtrate showed a peak with the same elution time as that of DEACM-OH and as the peak from the filtrate of $\text{NP}_{\text{TTA}}\text{-c}[\text{R}]\text{GdfK}$ irradiated with a 400 nm LED (Figure 5a). However, irradiation of a mixture of NP_{TTA} and free $\text{c}[\text{R}]\text{GdfK}$ with a 530 nm LED did not cleave DEACM from $\text{c}[\text{R}]\text{GdfK}$; only a peak with the same elution time as free $\text{c}[\text{R}]\text{GdfK}$ could be observed. These results show that the photocleavage reaction occurring in $\text{NP}_{\text{TTA}}\text{-c}[\text{R}]\text{GdfK}$ was mainly induced by TTA-UC through FRET. The time course of photorelease of DEACM from $\text{NP}_{\text{TTA}}\text{-c}[\text{R}]\text{GdfK}$ under continuous irradiation (Figure 5b), assessed by measuring the fluorescence of the filtrates (Supporting Information Figure 13), showed that 5 min of irradiation released around 75% of DEACM from $\text{NP}_{\text{TTA}}\text{-c}[\text{R}]\text{GdfK}$. In contrast, the filtrate of the nonirradiated $\text{NP}_{\text{TTA}}\text{-c}[\text{R}]\text{GdfK}$ showed relatively minimal release. The photocleavage profile of DEACM from $\text{NP}_{\text{TTA}}\text{-c}[\text{R}]\text{GdfK}$ was confirmed by HPLC (Supporting Information Figure 14).

When $\text{NP}\text{-c}[\text{R}]\text{GdfK}$ containing the photosensitizer PdOEP (but no DPA), termed $\text{NP}_{\text{PdOEP}}\text{-c}[\text{R}]\text{GdfK}$, were irradiated at 530 nm, DEACM was not cleaved from the micelles (Supporting Information Figure 15), which confirms that the photosensitizer alone could not transfer its energy to DEACM to cause photocleavage and 530 nm light irradiation could not directly cause photocleavage too. DPA does not absorb at 530 nm (Supporting Information Figure 16), so DPA alone could not have transferred the light energy to DEACM under irradiation at 530 nm.

Cell Binding Triggered by TTA-UC. Phototriggered binding of $\text{NP}_{\text{TTA}}\text{-c}[\text{R}]\text{GdfK}$ to cells by flow cytometry and confocal microscopy was studied with micelles in which a hydrophilic dye, Lissamine rhodamine B (LRB), was covalently bound to the PLA-PEG copolymer (forming PLA-PEG-LRB; Supporting Information Figure 17). LRB is photostable under irradiation with a 530 nm LED (150 mW cm^{-2}) for at least 10 min (Supporting Information Figure 18).

Human umbilical vein endothelial cells (HUVECs) and human glioblastoma (U87) cells, both of which express integrins including $\alpha_v\beta_3$ integrin,^{47,48} were incubated for 30

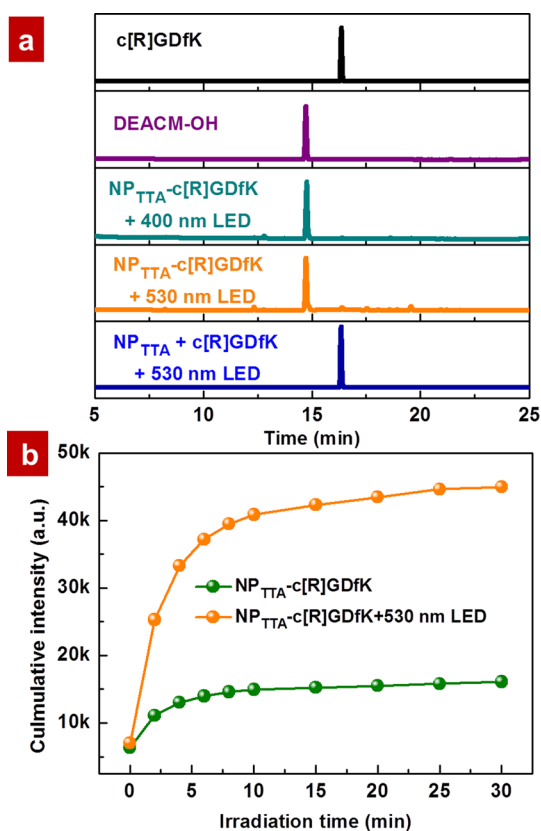


Figure 5. Photocleavage of DEACM from NP_{TTA}-c[R]GDfK by TTA-UC. (a) HPLC traces (detected at 390 nm) demonstrating photocleavage. For the bottom three traces, it was only the filtrates of the samples (i.e., not the micelles) that were tested by HPLC. (b) Cumulative fluorescent intensity (from integrated area under emission spectra; arbitrary units) of DEACM-OH photoreleased from NP_{TTA}-c[R]GDfK with 530 nm LED irradiation (150 mW cm⁻²) and in the dark.

min with the following micellar nanoparticles containing 10% PLA-PEG-LRB: NP_{TTA}-cRGDfK, NP_{TTA}, NP_{TTA}-c[R]GDfK, and NP_{TTA}-c[R]GDfK, the latter only irradiated with a 530 nm LED (150 mW cm⁻², 5 min). Cell-associated LRB fluorescence (a measure of particle binding) was measured by flow cytometry (Figure 6). HUVECs incubated with NP_{TTA}-cRGDfK exhibited 7.8-fold greater fluorescence than those exposed to ligand-missing NP_{TTA} (Figure 6a), indicating the ability of cRGDfK to target micelles to cells.⁴⁹ NP_{TTA}-c[R]GDfK exhibited little binding to cells, showing that the

caging group prevented ligand-mediated micelle binding to cells. Irradiation with a 530 nm LED (150 mW cm⁻², 5 min) increased cell binding of NP_{TTA}-c[R]GDfK by 3.3-fold. Similar results were obtained with U87 cells (Figure 6b). The results indicate that the DEACM caging group was cleaved from NP_{TTA}-c[R]GDfK by TTA-UC energy, revealing the cRGDfK on the micelle surface and allowing micelle binding to cells. The cell-associated fluorescence of HUVECs and U87 cells irradiated while incubated with NP_{TTA}-c[R]GDfK was less than that of cells incubated with NP_{TTA}-cRGDfK (Figure 6). This difference is attributable to the fact that both particle types contain the same % (w/w) of PLA-PEG-c[R]GDfK or PLA-PEG-cRGDfK but that with PLA-PEG-c[R]GDfK only 54.5% of polymers bore the peptide while with PLA-PEG-cRGDfK 96.6% bore the peptide.

Light-controlled micelle binding was further confirmed by confocal laser scanning microscopy (Supporting Information Figure 19). Irradiation with 530 nm LED (150 mW cm⁻², 5 min) induced cell binding and uptake of NP_{TTA}-c[R]GDfK in both HUVECs and U87 cells, while there was negligible binding and uptake of NP_{TTA} and nonirradiated NP_{TTA}-c[R]GDfK.

We have demonstrated a phototriggered targeting system using TTA-UC by loading a photosensitizer (PdOEP) and annihilator (DPA) into PLA-PEG polymeric micelles functionalized with DEACM-caged cRGDfK. Because of its hydrophobicity, the DEACM caging group was enclosed in the hydrophobic PLA core, so that the distance between DPA (donor) and DEACM (acceptor) was short, allowing FRET. Cell binding of this nanoparticle system was enabled by a short exposure (5 min) to a relatively low irradiance by a green light LED at 150 mW cm⁻². In contrast to other upconversion-based approaches where coherent light is required, TTA-UC can be triggered with noncoherent LED light. Given the limited tissue penetration by the wavelength of light used here, this particular TTA-UC system may be most relevant for applications where light can readily reach its target, as in ocular drug delivery. Research into methods to achieve excitation at longer wavelengths is currently the focus of considerable research interest.

■ ASSOCIATED CONTENT

📄 Supporting Information

Additional information and figures. The Supporting Information is available free of charge on the ACS Publications website at DOI: 10.1021/acs.nanolett.5b01325.

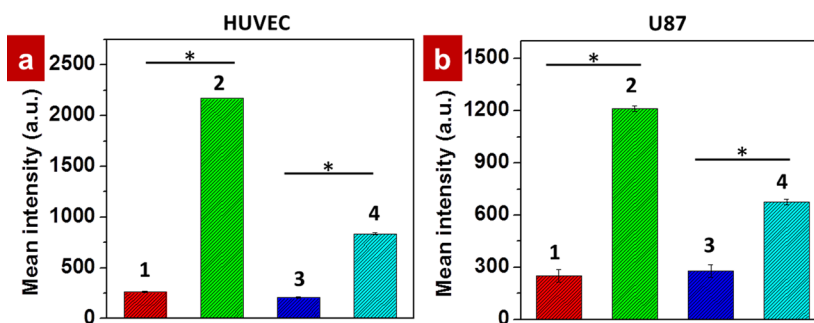


Figure 6. Flow cytometric analysis of cell binding and uptake of micelles. (1) NP_{TTA}, (2) NP_{TTA}-cRGDfK, (3) NP_{TTA}-c[R]GDfK, and (4) NP_{TTA}-c[R]GDfK irradiated with a 530 nm LED (150 mW cm⁻², 5 min) were incubated with HUVECs (a) or U87 cells (b) at 37 °C for 30 min. Cell fluorescence was then measured by flow cytometry. Data are means ± SD (*n* = 4), **p* < 0.001. All micelles were labeled with LRB.

■ AUTHOR INFORMATION

Corresponding Author

*E-mail: daniel.kohane@childrens.harvard.edu.

Author Contributions

W.W. and Q.L. contribute equally to this work. W.W., Q.L., and D.S.K. designed the project. W.W., Q.L., C.Z., A.B., T.Y., R.G.W., and P.A. performed the experiments. W.W., Q.L., A.B., and D.S.K. analyzed and interpreted the data. W.W., Q.L. and D.S.K. wrote the manuscript.

Notes

The authors declare no competing financial interest.

■ ACKNOWLEDGMENTS

This work was supported by NIH Grant GM073626 (to D.S.K.). We thank the Biopolymers & Proteomics Core Facility at the Koch Institute, the Flow Cytometry Core Facility at Dana-Farber Cancer Institute and the Harvard Medical School EM Facility for technical support. We thank Dr. Lisa Cameron at Dana-Farber Cancer Institute for her assistance with confocal laser scanning microscopy.

■ REFERENCES

- (1) Mills, J. K.; Needham, D. *Expert Opin. Ther. Patents* **1999**, *9* (11), 1499–1513.
- (2) Timko, B. P.; Dvir, T.; Kohane, D. S. *Adv. Mater.* **2010**, *22* (44), 4925–4943.
- (3) Dvir, T.; Banghart, M. R.; Timko, B. P.; Langer, R.; Kohane, D. S. *Nano Lett.* **2009**, *10* (1), 250–254.
- (4) Shamay, Y.; Adar, L.; Ashkenasy, G.; David, A. *Biomaterials* **2011**, *32* (5), 1377–1386.
- (5) Fan, N.-C.; Cheng, F.-Y.; Ho, J.-a. A.; Yeh, C.-S. *Angew. Chem., Int. Ed.* **2012**, *51* (35), 8806–8810.
- (6) Hansen, M. B.; van Gaal, E.; Minten, I.; Storm, G.; van Hest, J. C. M.; Lowik, D. J. *Controlled Release* **2012**, *164* (1), 87–94.
- (7) Yuan, Z. F.; Zhao, D.; Yi, X. Q.; Zhuo, R. X.; Li, F. *Adv. Funct. Mater.* **2014**, *24* (12), 1799–1807.
- (8) Barhoumi, A.; Wang, W.; Zurakowski, D.; Langer, R. S.; Kohane, D. S. *Nano Lett.* **2014**, *14* (7), 3697–3701.
- (9) Chien, Y.-H.; Chou, Y.-L.; Wang, S.-W.; Hung, S.-T.; Liao, M.-C.; Chao, Y.-J.; Su, C.-H.; Yeh, C.-S. *ACS Nano* **2013**, *7* (10), 8516–8528.
- (10) Kvam, E.; Tyrrell, R. M. *Carcinogenesis* **1997**, *18* (12), 2379–2384.
- (11) Barat, K. *Laser Safety: Tools and Training*, 2nd ed.; CRC Press: Boca Raton, FL, 2014.
- (12) Rumi, M.; Barlow, S.; Wang, J.; Perry, J.; Marder, S., Two-Photon Absorbing Materials and Two-Photon-Induced Chemistry. In *Photoresponsive Polymers I*; Marder, S., Lee, K.-S., Eds. Springer: Berlin, 2008; Vol. 213, pp 1–95.
- (13) Bort, G.; Gallavardin, T.; Ogden, D.; Dalko, P. I. *Angew. Chem., Int. Ed.* **2013**, *52* (17), 4526–4537.
- (14) Kachynski, A. V.; Pliss, A.; Kuzmin, A. N.; Ohulchanskyy, T. Y.; Bae, A.; Qu, J.; Prasad, P. N. *Nat. Photonics* **2014**, *8* (6), 455–461.
- (15) Barhoumi, A.; Salvador-Culla, B.; Kohane, D. S. *Adv. Healthcare Mater.* **2015**, DOI: 10.1002/adhm.201400768.
- (16) Wang, F.; Han, Y.; Lim, C. S.; Lu, Y. H.; Wang, J.; Xu, J.; Chen, H. Y.; Zhang, C.; Hong, M. H.; Liu, X. G. *Nature* **2010**, *463* (7284), 1061–1065.
- (17) Zhou, J.; Liu, Q.; Feng, W.; Sun, Y.; Li, F. *Chem. Rev.* **2015**, *115* (1), 395–465.
- (18) Roberts, S. T.; McAnally, R. E.; Mastron, J. N.; Webber, D. H.; Whited, M. T.; Brutchey, R. L.; Thompson, M. E.; Bradforth, S. E. *J. Am. Chem. Soc.* **2012**, *134* (14), 6388–6400.
- (19) Zhao, J. Z.; Ji, S. M.; Guo, H. M. *RSC Adv.* **2011**, *1* (6), 937–950.
- (20) Ceroni, P. *Chem.—Eur. J.* **2011**, *17* (35), 9560–9564.

- (21) Askes, S. H. C.; Bahreman, A.; Bonnet, S. *Angew. Chem., Int. Ed.* **2014**, *53* (4), 1029–1033.
- (22) Simon, Y. C.; Weder, C. *J. Mater. Chem.* **2012**, *22* (39), 20817–20830.
- (23) Liu, Q.; Yang, T.; Feng, W.; Li, F. *J. Am. Chem. Soc.* **2012**, *134* (11), 5390–5397.
- (24) Liu, Q.; Yin, B.; Yang, T.; Yang, Y.; Shen, Z.; Yao, P.; Li, F. *J. Am. Chem. Soc.* **2013**, *135* (13), 5029–5037.
- (25) Zhao, J.; Wu, W.; Sun, J.; Guo, S. *Chem. Soc. Rev.* **2013**, *42*, 5323–5351.
- (26) Singh-Rachford, T. N.; Castellano, F. N. *Coord. Chem. Rev.* **2010**, *254* (21–22), 2560–2573.
- (27) Kim, J.-H.; Deng, F.; Castellano, F. N.; Kim, J.-H. *Chem. Mater.* **2012**, *24* (12), 2250–2252.
- (28) Danhier, F.; Le Breton, A.; Preat, V. *Mol. Pharmaceutics* **2012**, *9* (11), 2961–2973.
- (29) Desgrosellier, J. S.; Cheresch, D. A. *Nat. Rev. Cancer* **2010**, *10* (1), 9–22.
- (30) Petersen, S.; Alonso, J. M.; Specht, A.; Duodu, P.; Goeldner, M.; del Campo, A. *Angew. Chem., Int. Ed.* **2008**, *47* (17), 3192–3195.
- (31) Lee, T. T.; García, J. R.; Paez, J. I.; Singh, A.; Phelps, E. A.; Weis, S.; Shafiq, Z.; Shekaran, A.; del Campo, A.; García, A. J. *Nat. Mater.* **2015**, *14*, 352–360.
- (32) Shembekar, V. R.; Chen, Y. L.; Carpenter, B. K.; Hess, G. P. *Biochemistry* **2007**, *46* (18), 5479–5484.
- (33) Furuta, F. Coumarin-4-ylmethyl Phototriggers. In *Dynamic Studies in Biology: Phototriggers, Photoswitches and Caged Biomolecules*; Goeldner, M., Givens, R., Eds.; Wiley-VCH: Weinheim, 2005; pp 29–55.
- (34) Klan, P.; Solomek, T.; Bochet, C. G.; Blanc, A.; Givens, R.; Rubina, M.; Popik, V.; Kostikov, A.; Wirz, J. *Chem. Rev.* **2013**, *113* (1), 119–191.
- (35) Jares-Erijman, E. A.; Jovin, T. M. *Nat. Biotechnol.* **2003**, *21* (11), 1387–1395.
- (36) Zhan, C.; Gu, B.; Xie, C.; Li, J.; Liu, Y.; Lu, W. *J. Controlled Release* **2010**, *143* (1), 136–142.
- (37) Murase, T.; Yoshihara, T.; Yamada, K.; Tobita, S. *Bull. Chem. Soc. Jpn.* **2013**, *86* (4), 510–519.
- (38) Babin, J.; Pelletier, M.; Lepage, M.; Allard, J. F.; Morris, D.; Zhao, Y. *Angew. Chem., Int. Ed.* **2009**, *48* (18), 3329–3332.
- (39) Wang, W. P.; Chau, Y. *Chem. Commun.* **2011**, *47* (37), 10224–10226.
- (40) Nasongkla, N.; Shuai, X.; Ai, H.; Weinberg, B. D.; Pink, J.; Boothman, D. A.; Gao, J. M. *Angew. Chem., Int. Ed.* **2004**, *43* (46), 6323–6327.
- (41) Haefele, A.; Blumhoff, J.; Khnayzer, R. S.; Castellano, F. N. *J. Phys. Chem. Lett.* **2012**, *3* (3), 299–303.
- (42) Boyer, J. C.; van Veggel, F. C. J. M. *Nanoscale* **2010**, *2* (8), 1417–1419.
- (43) Hagan, S. A.; Davis, S. S.; Illum, L.; Davies, M. C.; Garnett, M. C.; Taylor, D. C.; Irving, M. P.; Tadros, T. F. *Langmuir* **1995**, *11* (5), 1482–1485.
- (44) Tramier, M.; Zahid, M.; Mevel, J.-C.; Masse, M.-J.; Coppey-Moisan, M. *Microsc. Res. Technol.* **2006**, *69* (11), 933–939.
- (45) Duncan, R. R.; Bergmann, A.; Cousin, M. A.; Apps, D. K.; Shipston, M. J. *J. Microsc.* **2004**, *215* (1), 1–12.
- (46) Clegg, R. M., Förster resonance energy transfer-FRET what is it, why do it, and how it's done. In *Laboratory Techniques in Biochemistry and Molecular Biology*; Gadella, T. W. J., Ed.; Academic Press: Burlington, 2009; Vol. 33, pp 1–57.
- (47) Luscinskas, F. W.; Lawler, J. *FASEB J.* **1994**, *8* (12), 929–38.
- (48) Nakada, M.; Nambu, E.; Furuyama, N.; Yoshida, Y.; Takino, T.; Hayashi, Y.; Sato, H.; Sai, Y.; Tsuji, T.; Miyamoto, K. i.; Hirao, A.; Hamada, J. i. *Br. J. Cancer* **2013**, *108* (12), 2516–2524.
- (49) Zhang, F.; Huang, X.; Zhu, L.; Guo, N.; Niu, G.; Swierczewska, M.; Lee, S.; Xu, H.; Wang, A. Y.; Mohamedali, K. A.; Rosenblum, M. G.; Lu, G.; Chen, X. *Biomaterials* **2012**, *33* (21), 5414–5422.